Seven-phase axial and radial flux in-wheel machine with three active air gaps

Jinlin Gong, Benteng Zhao, Eric Semail, Ngac-Ky Nguyen, Youxi Huang

***Abstract* – For in-wheel machine, outer rotor machines appear as a natural solution. Practically these machines are either radial-flux with one rotor or axial-flux with two rotors. The paper is proposing a machine with three outer rotors with two different polarities in order to reduce useless end-windings while keeping an acceptable thickness for the radial-flux rotor and high torque quality. This Hybrid Flux Permanent Magnet original structure (named HFPM) is possible thanks to the use of seven phases. The third rotor can be considered as an option of an initial double-rotor axial-flux machine in order to increase the torque density. First, the machine structure and the winding design are presented; then, based on 3D finite element method, comparison between the two machines, with two or three rotors, are provided in terms of torque densities and qualities.**

***Index Terms*--axial flux, in-wheel machine, seven-phase machine, multi-phase machine, bi-harmonic machine**

I. INTRODUCTION

FOR in-wheel machine, outer rotor machines appear as a natural solution [1]. Practically these machines are either radial-flux with one rotor or axial-flux with two-rotors [2]. Radial-flux are classical and easy to make with stacked iron sheets but when the base speed is weak such as for bicycle or scooter applications [3], it is remaining unused space inside the stator [4] (Fig. 1 (a)) except with integrated drive such as a commercial e-bike machine [5], as shown in Fig. 1 (b). Axial-flux machine with two rotors (Fig. 2 (a)) are attractive to improve the compactness [6] [7]. Nevertheless, even if two rotors allow compensating globally the axial forces between stator and rotor, it is necessary to link together mechanically the two axial rotors in order to give sufficient mechanical strength.

The first idea of the paper is to make active this mechanical connection between the two axial rotors by transforming it into a third rotor as in [6] (Fig. 2 (b)), thus also making active part of the end windings. Unfortunately, when the number of poles is the same for this third rotor, the necessary thickness of the rotor yoke, in order to verify magnetic constraint of saturation, can be important [8] in comparison with a simple linking mechanical piece. As consequence, the second idea is to use a higher polarity for the radial-flux rotor while maintaining a high quality of torque as it is possible with multiphase machines [9] thanks to decoupling between harmonics.

Considering now the choice of the axial-flux configuration it is existing different solutions such as NN type slotted Torus machine (Torus-S) or NS type Torus-S [10], as shown in Fig. 3. The last one seems to be more attractive since the thickness of the stator is only determined by the depth of the slot and mechanical constraints for the rigidity of the stator [11]. In this case, 3-dimensionnal Soft Magnetic Composites (SMC) powder are difficult to use because of their weak mechanical properties. Costly enrolled iron sheets are more adapted. On contrary NN type Torus-S stator thickness is constrained by the magnetic polarity of the axial rotor: large unnecessary end-windings can be then induced [12]. In this paper, the third rotor makes active the end-windings: the stator thickness is then less a drawback. Moreover, low-cost material with modest mechanical properties such as SMC powder can be advantageously used.

In the paper, the machine structure and the winding design are first presented; then, based on 3D finite element method, the initial machine with two axial rotors is compared to the proposed three-rotor machine.

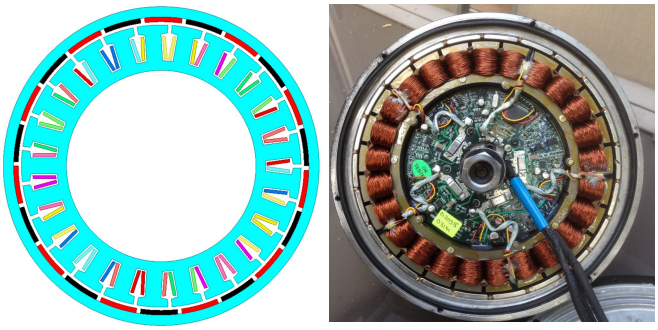

(a)] (b)

Fig. 1. radial flux with one rotor and useless center space (a) and associated commercial integrated outer- radial-flux 5-phase machine for bicycle (b) [5]

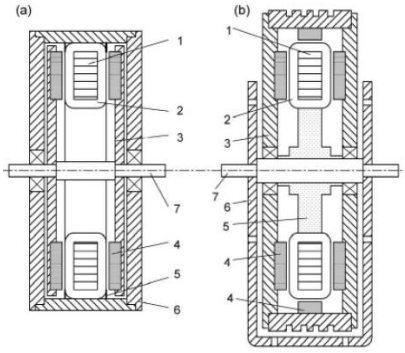

Fig. 2. Outer rotor PM machine from [6] (3/iron-4/magnets)), (a) two-axial rotors, (b) with a supplementary radial-flux rotor

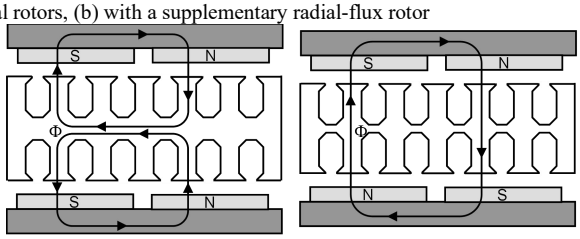

Fig. 3. Two different topologies for TORUS-S Axial Flux Permanent Magnet machines left NN type , right NS type [10]

II. TOPOLOGY, WINDING DESIGN AND PROTOTYPE

A. *Machine topology*

The proposed machine with NN type Torus-S structure is shown in Fig. 4, including the 1/4 of the structure in Fig. 4 (a) and the exploded structure of the whole machine in Fig. 4 (b). It is a sandwich structure i.e. two outer rotors with PMs surface-mounted and one stator with toroidal tooth concentrated winding. By adding a third radial rotor, the upper end-windings of this NN-type Torus-S structure become active with an even greater contribution as is the axial length of the stator core made of SMC material. In order to enhance the torque density and power density, the radial rotor with V-shape magnets is designed. Moreover, the number of poles of the radial rotor is 36, i.e. 3 times more than the other two axial-flux rotors with 12 poles. This choice is possible keeping a high torque quality by using a machine with seven phases thanks to the decoupling between the first and third harmonics. The characteristics of this particular machine will be investigated the following section.

B. *Non-overlapping winding design*

The first constraint imposed to the toroidal windings of the machine is the making simplicity: a tooth concentrated winding without overlapping is chosen. As consequence, the winding is then often a fractional slot concentrated winding (FSCW) [13] whose main challenges is the rich content of space harmonics of magneto-motive force (mmf), including both sub- and high- orders. These parasite spatial harmonics can lead to eddy current losses, vibration and noise, local core saturation etc., which deteriorate the performance of the machine. It is necessary to choose carefully the slot/pole combination in order to avoid these drawbacks.

Two criteria are used to select the slot/pole combination of the proposed machine:

- The first one is the high value of winding factor, which is related to the torque density. Due to the specificity of the machine, the winding factors of both the fundamental and the third harmonic are expected to be important.
- The second one is the content of the parasitic harmonics of mmf under the current injection of both the fundamental and the third harmonic.

Considering the first criterion, 14-slot/12-pole combination is selected [17]. The winding factors of the fundamental and the third harmonic are 0.97 and 0.78 respectively. The mmf spectrum is then analyzed and presented in Fig. 5. As it can be seen, the working harmonic is the 6th with the fundamental current supply, and the 18th with the 3rd harmonic current. Unfortunately, the parasitic harmonics of mmf are rich, especially the ones with big value of magnitude, such as the 8th and the 20th. In order to reduce the negative effects induced by the parasitic harmonics, stator shift technique is applied [14]. A novel winding topology with 28-slot/12-pole combination is achieved. It can be noted that in Fig. 5, the mmf spectrums under the injection of both the fundamental and the 3rd harmonic are improved. Meanwhile, the winding factors are also with the same high value, i.e. K_1=0.97 and and K_3=0.78. Therefore, a higher torque density is expected.

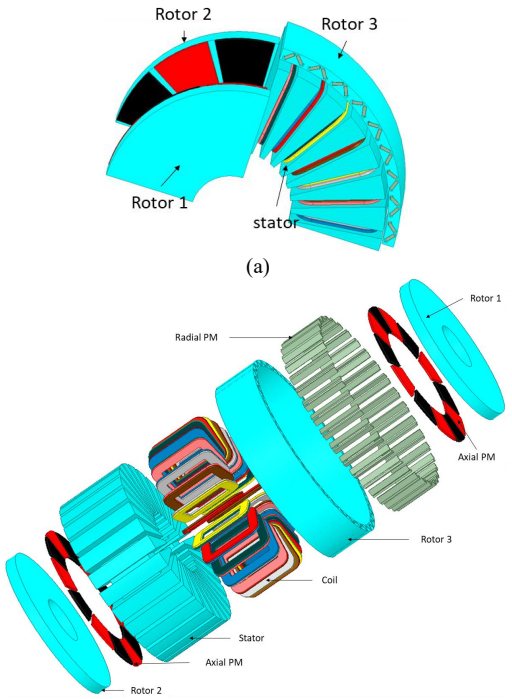

Fig. 4. Hybrid Flux Permanent Magnet (HFPM) machine topology with (a) 1/4 structure and (b) exploded structure

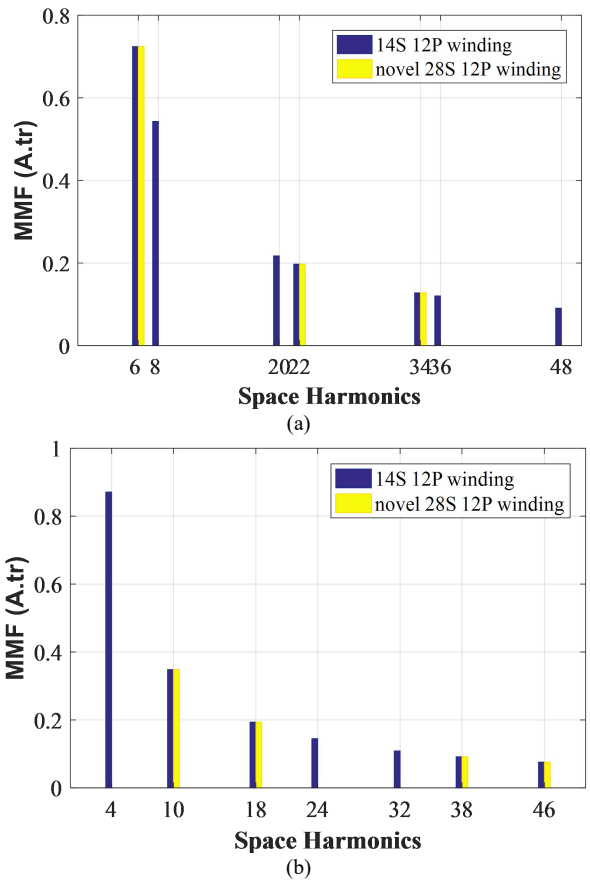

Fig. 5. mmf harmonic spectrum with injection of (a) fundamental current (b) 3rd harmonic of current

Fig. 6 shows the novel winding topology. The coils of the same color belong to the winding of the same phase. It is toroidal type and the non-overlapping one, even with stator shift technique application.

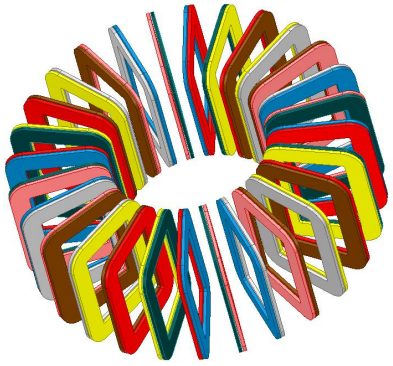

Fig. 6. Novel 28-slot/12-pole winding topology

C. *Prototype specifications*

Fig. 7 shows the SMC stator core and the third laminated radial rotor of the prototype. The back iron of the two axial rotors are made of non-laminated iron 1010 and the third radial rotor is laminated with sheets.

Fig. 8 shows the B-H curves of three magnetic materials used for the prototype: SMC, laminated sheets, and 1010 iron. It can be seen that the difference of magnetic property of the three materials is important. The low cost SMC material is characterized with low values both in permeability and saturation flux density. Therefore, the axial length of the stator with SMC is greater than that with enrolled iron sheets.

(a) (b)

Fig. 7. Prototype with (a) Stator in SMC and (b) laminated radial rotor

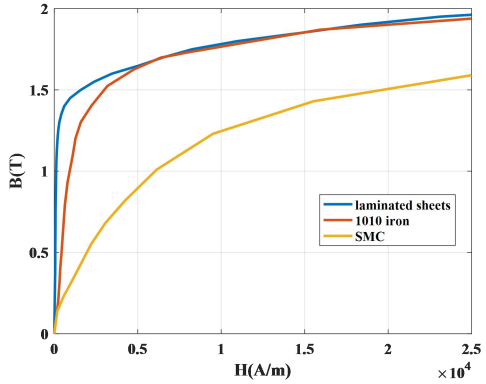

Fig. 8. B-H curves of three materials

The parameters and the machine dimensions are shown in table I.

TABLE I PARAMETER AND MACHINE DIMENSIONS

Number of phases	7
Number of slots	28
Number of pairs of poles (axial rotors) p	6
Number of pairs of poles (radial rotors) 3p	18
Stator core outer diameter (mm)	145.9
Stator core inner diameter (mm)	50.6
Slot dimension (mm)	4.3*13.1
Number of wires per slot	22
Axial length of stator core (mm)	47.6
Axial length of axial rotor core (mm)	5.3
thickness of axial magnet (mm)	1.9
thickness of air gaps (mm)	1
Outer diameter of radial rotor (mm)	183.54
Inner diameter of radial rotor (mm)	161
Axial length of the radial rotor (mm)	47.6
Thickness of V-shape magnet (mm)	2
Nominal speed (rpm)	600
Nominal torque (Nm)	8

III. MATHEMATICAL MODEL

Neglecting saturation and reluctance effects, the seven-phase machine can be considered as three two-phase fictitious machines and one single-phase machine magnetically decoupled [15]. Each fictitious machine is characterized by a set of harmonics as shown in Table II. Under assumption of no reluctance effect, the fictitious machines are magnetically independent, however they are mechanically linked together, i.e. the total output torque of the machine is the sum of the fictitious machines. It should be noted that the zero-sequence machine is not taken into account when the machine is wye connected.

TABLE II THE HARMONICS CORRESPONDING TO FICTITIOUS MACHINES

Fictitious machine	Associated odd harmonics
Primary machine called M1	1,13,15,27 …7*k±1
Secondary machine called M5	5,9,19,23 …7*k±2
Third machine called M3	3,11,17,25 …7*k±3
Zero-sequence machine	7, 21, …, 7*k

A. *Electromagnetic torque expression*

The electromagnetic torque of the seven-phase machine is derived in this part, using fictitious machines approach [12] with the formula (1).

$$T_{em} = \frac{\overrightarrow{e_{M1}}\overrightarrow{i_{M1}} + \overrightarrow{e_{M3}}\overrightarrow{i_{M3}} + \overrightarrow{e_{M5}}\overrightarrow{i_{M5}}}{\Omega} \quad (1)$$

where Ω is the rotating speed of the rotor in rad/s; $\overrightarrow{e_{Mk}}$ and $\overrightarrow{i_{Mk}}$ are back-emf and current vectors of fictitious machine M_k with k=1, 3, 5. They are obtained by vector projection of back-emf and current vectors in the associated planes of each fictitious machine, defined by the classical Concordia transformation.

In each fictitious machine, it can be considered that only the main harmonic is contributing significantly to the torque. As consequence the expression of the electromotive force in each fictitious machine can be approximated by:

$$\overrightarrow{e_{Mk}} = \sqrt{\frac{7}{2}} E_k \sqrt{2}\left(-\sin(kp\theta)\overrightarrow{x_{\alpha k}} + \cos(kp\theta)\overrightarrow{x_{\beta k}}\right) \quad (2)$$

with E_k the RMS value of the harmonic k of back-emf.

As the adopted strategy chosen for the supply in the design step is classically MTPA (Maximum Torque Per Ampere), the vector current is co-linear with the back-emf vector. The vector current is then:

$$\overrightarrow{i_{Mk}} = \sqrt{\frac{7}{2}} K_0 \; E_k \sqrt{2}\left(-\sin(kp\theta)\overrightarrow{x_{\alpha k}} + \cos(kp\theta)\overrightarrow{x_{\beta k}}\right) \quad (3)$$

By (1), the obtained torque with three injected harmonics is then:

$$T = 7K_0E_1^2\left(1+(E_3/E_1)^2+(E_5/E_1)^2\right)/\Omega \quad (4)$$

And the value of K_0 is linked to the A_L linear current density chosen for the design of the machine.

B. V-shape PM machine modeling

In order to reinforce the flux density in the air gap and improve the flux-weakening capability, the radial rotor is designed using V-shaped poles. An equivalent magnetic circuit using Thevenin's theorem [16] is therefore built for the modeling of the radial rotor, as shown in Fig. 9.

In Fig. 9, R_{tr}, R_{ts}, R_{ys}, R_{yr} are related to the reluctance of stator and rotor teeth and yokes; R_g is the reluctance of the air gap; R_b is the reluctance of flux barriers; R_{Fe} is the reluctance of the saturated iron bridges under one pole. Using Thevenin-equivalent theory, the following relationship can be obtained:

$$F_{th} = F_m - R_{th}\Phi_{sat} \quad (5)$$

Where F_{th} is the equivalent Thevenin mmf; F_m is the mmf generated from PMs; R_{th} is equivalent Thevenin reluctance which can be obtained by the sum of PMs reluctance and internal airgap around the PMs; Φ_{sat} is the flux required to saturate the iron bridges which can be calculated as follows,

$$\Phi_{sat} = B_{sat} w_{Fe} k_f L \quad (6)$$

Where B_{sat} is the flux density in saturated iron and K_f is the stacking factor for the iron lamination; L is the axial length of the magnet; w_{Fe} is the sum of the iron bridge widths under one pole.

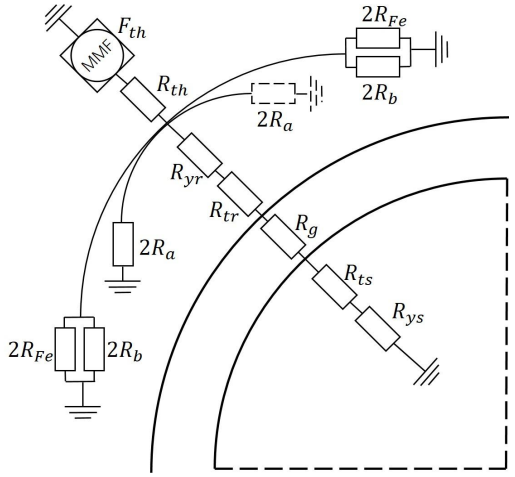

Fig. 9. Equivalent magnetic circuit based on Thevenin theorem

IV. 3D FINITE ELEMENT MODEL ANALYSIS

A. Flux density distribution

The 3D-FEM is used to validate the pre-design of the HFPM machine. In order to reduce computation time, 1/4 of machine model is built and analyzed. The generated mesh and the flux density distribution under no-load condition is shown in Fig. 10. As can be seen, in the stator core and the two axial rotors, the maximum of magnetic flux density is about 1.6T. In the radial rotor, the iron bridge is saturated and the maximum value of the magnetic flux density is 2T.

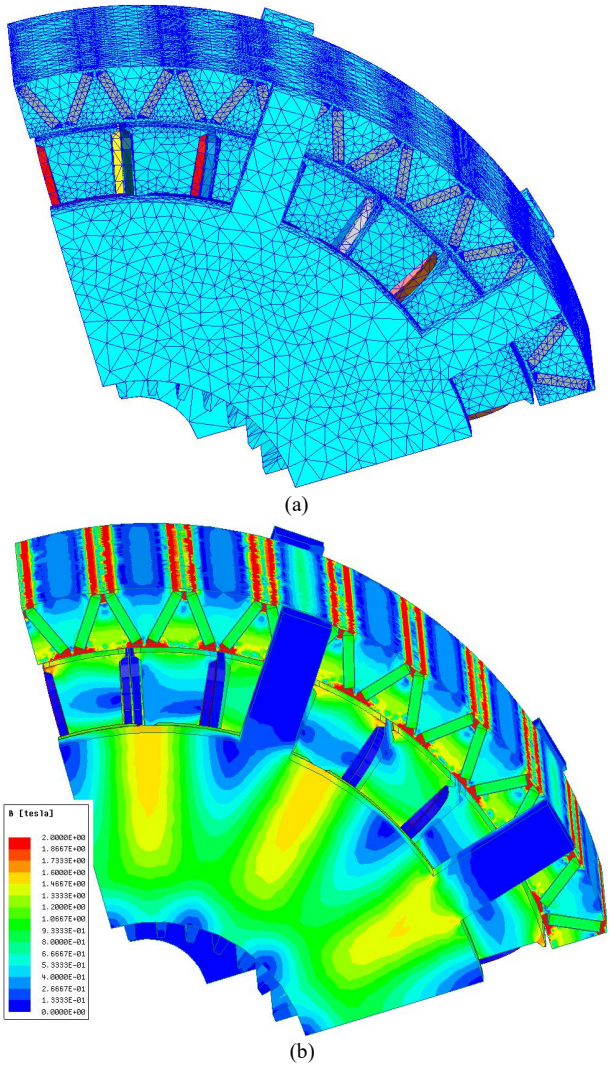

Fig. 10. 3D FEM analysis results with (a) mesh generation and (b) flux density distribution of HFPM machine

B. Flux Linkage

Fig. 11 shows the flux linkage and its harmonic spectrum of one phase in no-load condition. It can be noted that the 1st and the 3rd harmonic component are dominant. The ratio between them Φ_3/Φ_1 is equal to 0.41. The other harmonics, such as the 5th and the 9th harmonics, are both of very small magnitude and can be neglected in the following analytical analysis.

C. Cogging Torque

Fig. 12 shows the 3D-FEM predicted cogging torque, in which the red curve is related to the proposed 3-rotor HFPM machine. The blue curve is related to the initial machine called AFPM obtained by suppressing the magnets of the third radial rotor of HFPM. It can be seen that the cogging torque is increased by adding the magnet in the 3rd radial rotor, however, they are both small values (less than 6% for HFPM and 3% for AFPM) in comparison with the rated torque value.

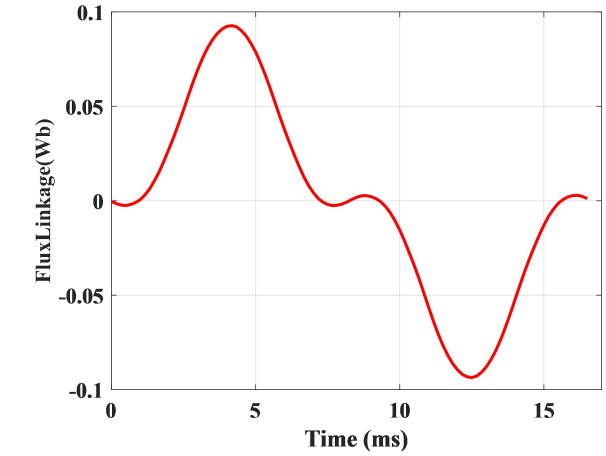

(a)

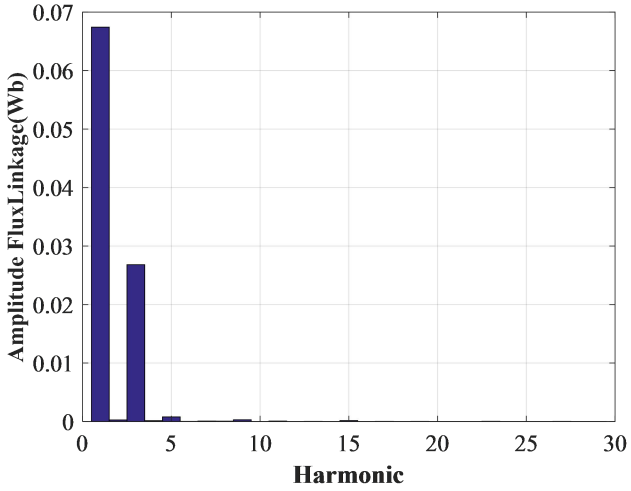

(b)

Fig. 11. FE validation of HFPM machine at 600 rpm with (a)Flux linkage (b) harmonics

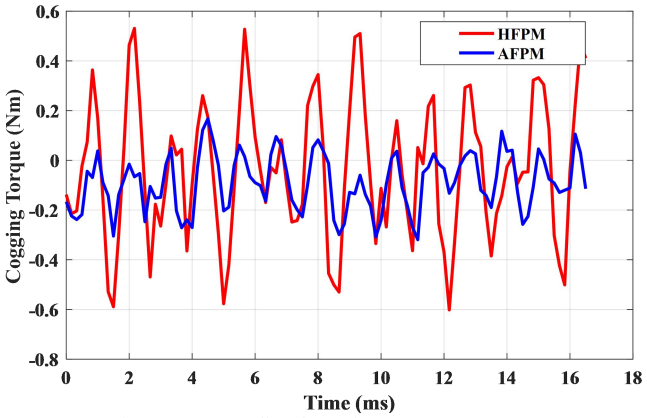

Fig. 12. FE predicted cogging torque at 600 rpm

D. *Electromagnetic Torque*

As it can be considered that the flux linkage contains only the first and third harmonic, only the first and third harmonics of current are injected. For a given RMS value of current, a comparison of the torques obtained with MTPA strategy as presented in III-A is made considering three kinds of supply: with only the first, only the third, and both the first and the third sinusoidal currents as shown in Fig. 13. It can be remarked that the peak value of the currents is of same order. The waveforms of the torque at 600 rpm speed are then shown in Fig. 14. The torque ripples can be considered as low even when two harmonics of close amplitudes are injected (about 6 %), and the main frequency of the pulsation is 840Hz as expected (14*p*600/60). It confirms that the first and third harmonic interactions are weak because of the orthogonality of the two "αβ" planes associated to these two harmonics. Thanks to (4) and for the considered seven-phase machine whose Φ_3/Φ_1=0.4, the torque under bi-harmonic current supply is 53% (resp. 26%) higher than this one obtained with only the first (resp. the third) harmonic current: the global torque is the sum of the torques produced in each "αβ" plane. With a same level of copper losses and about same peak current, the bi-harmonic supply is obviously interesting.

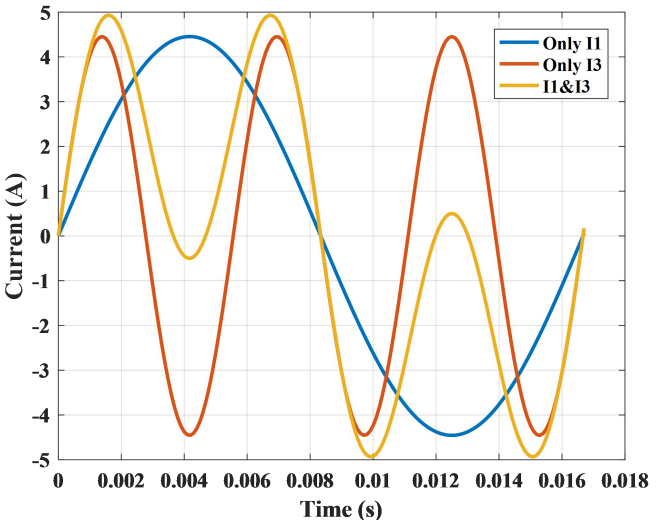

Fig. 13. For a given RMS current, phase currents for the MTPA supplies at 600 rpm (62.8rd/s) with a period of 15.9ms for the first harmonic

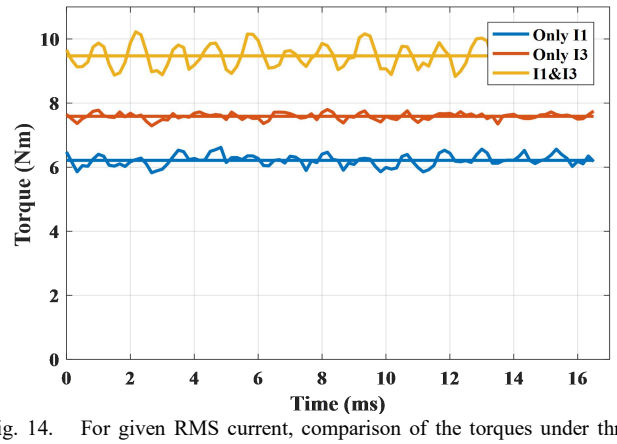

Fig. 14. For given RMS current, comparison of the torques under three kinds of supply: only the first, only the third, and both the first and the third harmonic current at 600 rpm (62.8 rd/s)

V. PERFORMANCE COMPARISON

The performance of the HFPM machine is compared to the AFPM machine presented in IV-C.. Fig. 15 shows the comparison of back-EMF at no-load. It can be seen that the amplitudes of the 3rd harmonic back-EMF for the HFPM machine are significantly increased, 5 times higher than the one of AFPM. However, the fundamental component is slightly reduced 5%, due to the saturation of the SMC material with the addition of the 3rd radial rotor.

Table III shows the volume, mass, volume of magnet, volume torque density in volume, and the mass torque

density.

Under the same 3.15A RMS current injection, the output torque of the HFPM is increased by 51% under bi-harmonic current supply, as shown in Fig. 16 (a). As consequence, the torque densities in volume and in mass are both significantly improved by 50% and 54%, as shown in Fig. 16 (b). The main drawback is a higher cost because of the addition of magnets. The third rotor can be considered as an option to increase easily the torque keeping the same volume of the machine.

TABLE III IMPACT OF ADDITION OF MAGNETS IN THE THRID RADIAL ROTOR

Machine	Volume (dm^3)	Mass (kg)	Volume magnet (dm^3)	Torque N.m)	Torque density (Nm/m^3)	Torque density (Nm/kg)
AFPM	1.693	9.21	0.03	6.3	3721	0.68
HFPM	1.693	9.01	0.10	9.5	5595	1.05
Variation (%)	0	-2	+233	+51	+50	+54

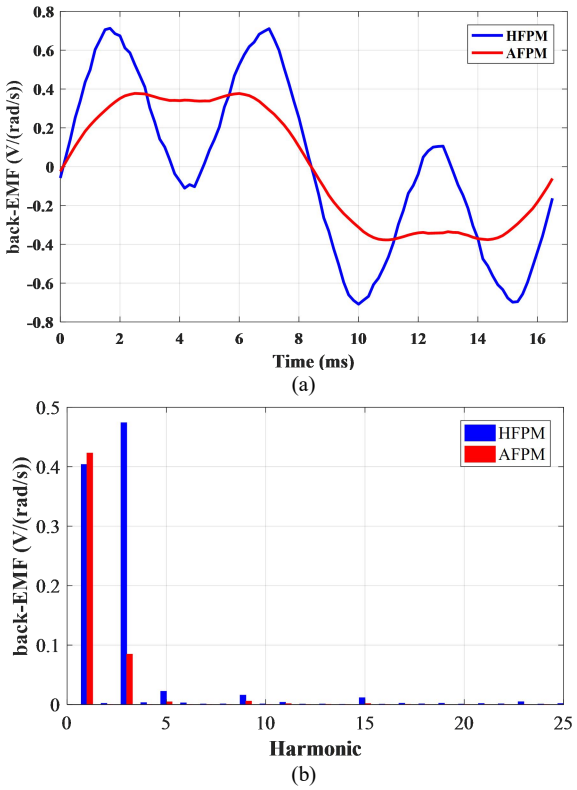

Fig. 15. Comparison of back-EMF with (a) curves and (b) spectrum

VI. CONCLUSION

In this paper, by simply adding magnets inside a mechanical linking between two axial rotors of a 7-phase axial flux permanent magnet machine, a hybrid flux permanent magnet machine is obtained. Using specific property of multiphase machine, the chosen number of poles of the third radial rotor is three times this one of the two other axial rotors: the corresponding small thickness of this third radial allows to increase by more than 50% mass and volume torque densities. It is then possible to propose two machines with many identical components and whose geometry and mass are similar but whose performances are quite different. As example of application, two versions of a scooter could be then easily obtained with only a different quantity of Permanent Magnets inside. Results have been only presented for MTPA strategy. The degrees of freedom of the machine for torque production allow other strategies. Flux weakening capabilities will be studied in next paper.

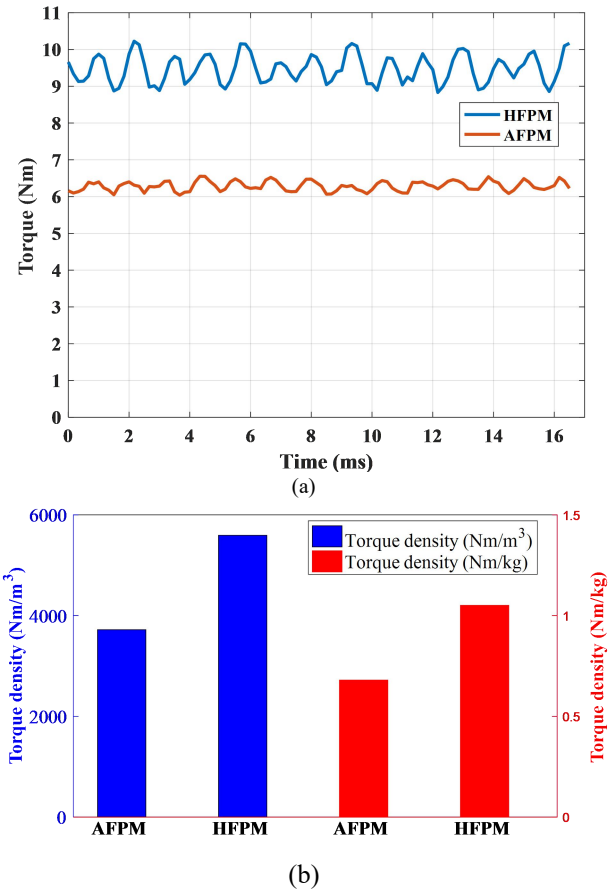

Fig. 16. for a given RMS current, performance comparison with (a) torque and (b) torque densities of both SMC-stator and PM rotors machines with MTPA strategy

VII. REFERENCES

[1] J. B. Wang, K. Atallah, Z. Q. Zhu, and D. Howe, "Modular three-phase permanent-magnet brushless machines for in-wheel applications," *IEEE Trans. Veh. Technol.*, vol. 57, no. 5, pp. 2714-2720, Sep. 2008.

[2] C. J. Ifedi, B. C. Mecrow, S. T. M. Brockway, G. S. Boast, G. J. Atkinson, and D. K. Perovic, "Fault-tolerant in-wheel motor topologies for high-performance electric vehciles," *IEEE Trans. Ind. Appl.*, vol. 49, no. 3, pp. 1249-1257, May/June, 2013.

[3] Y. Yang, M. M. Rahman, T. Lambert, B. Bilgin, and A. Emadi, "Development of an External Rotor V-Shape Permanent Magnet Machine for E-Bike Application," *IEEE Trans. Energ. Conv.*, vol. 33, no. 4, pp. 1650-1658, Dec. 2018.

[4] H. Zhang, W. Hua, D. Gerada, C. Gerada, Y. Li, G. Zhang, "Comparative Study on Two Modular Spoke-Type PM Machines for In-wheel Traction Applications," *IEEE Trans. Energ. Conv.*, vol. 34, no. 4, pp. 2137-2147, Dec. 2019.

[5] R. K. Dhawan, A. VA, "Multi-Phase Multi-Pole Electric Machine," U.S. Patent 20130257327A1, Oct. 3, 2013.

[6] J. F. Gieras, R-J. Wang, M. J. Kamper, *Axial Flux Permanent Magnet Brushless Machines*, USA: Kluwer Academic Publishers, 2004.

[7] A. Hemeida, M. Taha, A. A.-E. Abdalh, H. Vansompel, L. Dupré, P. Sergeant, "Applicability of Fractional Slot Axial Flux Permanent Magnet Synchronous Machines in Field Weakening Region, " *IEEE Transactions on Energy Conversion*, vol. 32, no. 1, March 2017, pp.111-121.

[8] Z. Zhu, Y. Huang, J. Dong, F. Peng, "Investigation Study of the Influence of Pole Numbers on Torque Density and Flux-weakening

Ability of Fractional Slot Concentrated Winding Wheel-Hub Machines, " *IEEE Access*, vol. 7, June 2019, pp.84918-84928.
[9] J. Gong, H. Zahr, E. Semail, M. Trabelsi, B. Aslan, F. Scuiller, "Design Considerations of Five-Phase Machine with Double p/3p Polarity, " *IEEE Transactions on Energy Conversion*, vol. 34, no. 1, March 2019, pp.12-24.
[10] M. Adyn, S. Huang, T.A. Lipo, "Axial Flux Permanent Magnet Disc Machines: A Review," University of Wisconsin-Madison, College of Engineering, Wisconsin Power Electronics Research Center, 2004.
[11] B. Zhang, T. Seidler, R. Dierken, and M. Doppelbauer, "Development of a Yokeless and Segmented Armature Axial Flux Machine," *IEEE Transactions on Industrial Electronics*, vol. 63, no. 4, April 2016, pp.2062-2071.
[12] F. Locment, E. Semail, X. Kestelyn, "Vectorial approach-based control of a seven-phase axial flux machine designed for fault operation," *IEEE Trans. Indus. Electr.*, vol. 55, no. 10, October 2008, pp. 3682-3691.
[13] A. M. El-Refaie, "Fractional slot concentrated windings synchronous permanent magnet machines: opportunities and challenges," *IEEE Trans. Indus. Electr.*, vol. 57, no. 1, Jan. 2010, pp. 107-121.
[14] P. B. Reddy, K. K. Huh, and A. M. EL-Refaie, "Generalized Approach of Stator Shifting in Interior Permanent-Magnet Machines Equipped With Fractional-Slot Concentrated Windings," *IEEE Trans. on Ind. Electronics.*, vol. 61, no. 9, Sep. 2014, pp. 5035-5046.
[15] E. Semail, X. Kestelyn, and A. Bouscayrol, "Right harmonic spectrum for the back-electromotive force of an n-phase synchronous motor," in *Conference Record of the 2004 IEEE Industry Applications Conference, 2004. 39th IAS Annual Meeting*, Seattle, WA, USA, 2004, vol. 1, pp. 1-8.
[16] P. Thelin, H. P. Nee, "Analytical calculation of the airgap flux density of PM synchronous motors with buried magnets including axial leakage, tooth and yoke saturations," in *Eighth International Conference on Power Electronics and Variable Speed Drives,* London, UK, Sept. 2004, pp. 1-6.
[17] B. Aslan, E. Semail, J. Korecki, J. Legranger, "Slot/Pole Combinations Choice for Concentrated Multiphase Machines Dedicated to Mild-Hybrid Applications," in *Proc. 37th Annual Conference on IEEE Industrial Electronics Society (IECON)*, Vienna, Austria, Nov. 10-13, 2013, pp 3698 – 3703.

VIII. BIOGRAPHIES

Jinlin Gong (M'13) received the Ph. D degree in electrical engineering from Ecole Centrale de Lille, France, in 2011. From October 2011 to August 2012, he was an assistant professor at the Engineering School of Arts et Métiers ParisTech, Lille, France. He is currently associate professor of the School of Electrical Engineering of Shandong University, Jinan, China. His research interests include optimal design and control of linear motors and multiphase motors.

Benteng Zhao graduated from Shandong University of Science and Technology, Qingdao, China, in 2017 and is currently a master student at the School of Electrical Engineering of Shandong University, Jinan, China. He specializes in motors and electrical appliances. His area of interest is design, modeling and simulation of multiphase machine.

Eric Semail (M'02) graduated from the Ecole Normale Supérieure, Paris, France, in 1986, received the Ph.D. degree in 2000 and became in 2010, full Professor of Arts et Metiers Institute of technology Lille, France in laboratory of Electrical Engineering of Lille (L2EP). His fields of interest include design, modeling, and control of multiphase electrical drives (converters and ac drives)

Ngac-Ky Nguyen (M'13) received the B.Sc. degree in electrical engineering from Ho Chi Minh City University of Technology, Ho Chi Minh, Vietnam, in 2005, and the Ph.D. degree in electrical and electronic engineering from the University of Haute Alsace, Mulhouse, France, in 2010. Since September 2012, he has been an Associate Professor with the Laboratory of Electrical Engineering and Power Electronics of Lille, Arts et Metiers ParisTech, Lille, France. His research interests include modeling and control of synchronous motors, power converters, fault-tolerant control and fault diagnosis of multiphase drives.

Youxi Huang received the B.S. degree from North China Electric Power University in 2019. He is currently a master student in School of Electrical Engineering, Shandong University of China. His current research interests include electrical machines control.